

## PAPER

## An experimental study of ultrasonic imaging with a reduced number of array elements using the envelope method

Takuya Sakamoto\*, Hirofumi Taki and Toru Sato

Graduate School of Informatics, Kyoto University

(Received 18 October 2010, Accepted for publication 26 March 2011)

**Abstract:** In this experimental study, we conducted measurements using a 128-element ultrasonic array system. Ultrasonic images generated by the conventional migration method were compared with the Envelope method, a promising high-resolution imaging technique. To determine the image quality of an ultrasonic measurement system that uses fewer elements, we selected 64, 32, 16 and 8 elements from the total 128 elements used in our imaging process. The results show that in homogeneous environments the Envelope method can produce clearer images than those produced by the conventional method even when using a small number of elements, suggesting that the introduction of the Envelope method could be an effective way of reducing the number of elements employed in array systems, while maintaining high image quality.

**Keywords:** Ultrasound CT, Envelope method, Ultrasound, Medical imaging

**PACS number:** 43.35.Wa [doi:10.1250/ast.32.143]

### 1. INTRODUCTION

Medical ultrasonic imaging is of great interest because of its wide range of clinical applications. In particular, estimating the shape of a surface is an important application, and includes monitoring of the development of an embryo [1], the evaluation of cardiac function [2] and monitoring of gas and fluid flow in a vessel [3]. These studies scan the ultrasound probe manually or mechanically to obtain high-resolution images. The introduction of an element array is indispensable to the improvement of imaging capability in terms of resolution and frame rate.

Imaging by ultrasound computer tomography (CT) is considered an attractive alternative to X-ray CT. The ultrasound CT technology employs element arrays to achieve high-resolution imaging, and offers safe and non-invasive medical imaging compared with X-ray CT [4–8]. In general, an array probe with a large number of elements is required to achieve better image quality. However, it is not easy to implement a large-scale element array because of its high cost, which has been a major factor inhibiting its wider application within the field of medical ultrasound imaging [9]. To resolve this problem, sparse array technology has been studied [10–12]. By randomly eliminating some elements, sparse arrays can reduce the number of elements while maintaining sharply focused

beams. In this paper, we propose another method of reducing the number of elements by addressing on the signal processing aspect of the ultrasound imaging.

In the field of ultra wide-band radar imaging, an accurate imaging technique known as the Envelope method has been proposed [13] for the imaging of a simplified target model with a clear boundary placed in relatively homogeneous media. The high performance of the Envelope method with ultra wide-band radar systems has been confirmed through experimental studies [14,15]. Saho *et al.* presented the results of applying the Envelope method to ultrasonic measurement data [16], in which the transmitting and receiving elements were installed on a robotic arm to enable mechanical scanning. Unfortunately, the Envelope method was specifically developed for a linear element array, and not for other array layouts such as the concave array, which is more suitable for most medical ultrasound imaging devices [17,18].

Helbig *et al.* reported on an imaging method for a concave element array [19], and introduced an extended version of the SEABED method [20], a well known high-speed imaging algorithm. Although the SEABED method is similar to the Envelope method, it has been reported that the Envelope method is more robust for noisy data than the SEABED method [13]. Consequently, there appears to be promising potential for obtaining better imaging performance by developing an extended version of the Envelope method for use with concave arrays.

---

\*e-mail: t-sakamo@i.kyoto-u.ac.jp

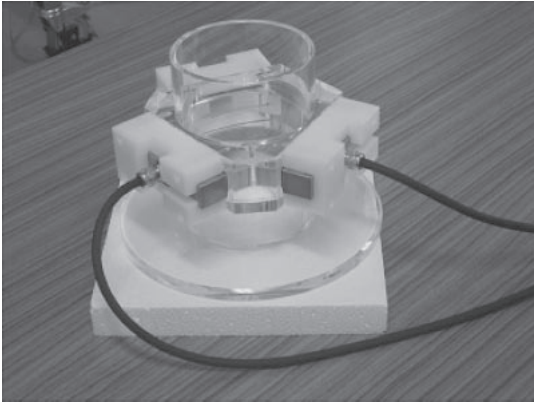


Fig. 1 Ultrasonic imaging experimental system.

In this paper, we extend the original Envelope method so that it can be applied to concave arrays, and apply the extended Envelope method to ultrasonic experimental data measured with three 128-element concave arrays. The aim of this work is to demonstrate that the extended Envelope method produces high-quality images compared with the conventional migration method, and to verify that the image quality does not deteriorate when employing the extended Envelope method when using a small number of elements.

## 2. SYSTEM MODEL

The measurement system for the ultrasonic imaging experiment is shown in Fig. 1. For simplicity, we employ a 2-dimensional experimental setup. We positioned three 128-element arrays around a water tank. The elements of each array are spaced at intervals of 0.6 mm along a circle with a diameter  $r_0$  of 50 mm. The array aperture is  $127 \times 0.6 \text{ mm} = 76.2 \text{ mm}$ , which corresponds to an angular spread of  $87.3^\circ$  in the circular water tank. The experimental setup and the definition of the spatial coordinates is shown in Fig. 2, where the first element #1 of the array is located on the  $x$ -axis. An acrylic circular cylinder is located at the  $x - y$  coordinates, (1.1 mm,  $-2.0 \text{ mm}$ ) in the water tank. Double-cycle pulses with a center frequency of 2.0 MHz are transmitted from each element; the echoes are received by the same element sequentially as in Fig. 3, essentially forming a mono-static measurement system. For each element array, a total of 128 signals are received in the time domain. These signals are first stored in memory and then processed to produce images of the target.

We define  $\mathbf{r}_i$  ( $i = 1, 2, \dots, 128$ ) as the position of the  $i$ -th element of each array. The signal  $s_i(t)$  is the echo associated with the  $i$ -th transmitting and receiving element. Received signals  $s_i(t)$  are processed with a matched filter that is designed to be matched to the transmitted waveform. In this paper, we use a filter with an impulse response  $p(t)$  given by

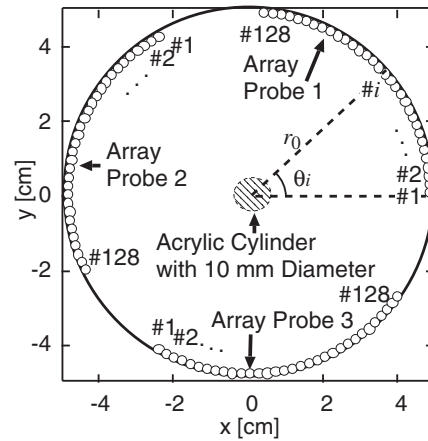


Fig. 2 Experimental system setup with an acrylic cylinder.

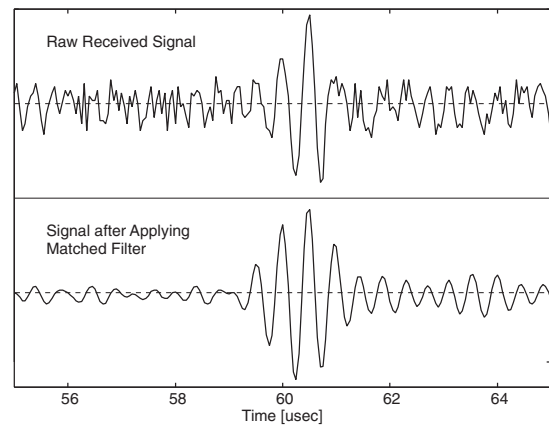


Fig. 3 A received signal with and without matched filtering.

$$p(t) = \exp(-t^2/2\sigma^2) \cos(2\pi ft), \quad (1)$$

where  $\sigma = 0.4 \mu\text{sec}$  and  $f = 2.0 \text{ MHz}$ . Figure 3 shows a signal measured by the experimental system with and without applying the matched filter. After applying the matched filter, the signal has a higher signal-to-noise ratio (S/N) and the waveform becomes more symmetrical.

## 3. IMAGING METHODS

### 3.1. Migration Method

The migration method is often used for medical imaging where the image  $S(\mathbf{x})$  is calculated as

$$S(\mathbf{x}) = \left| \sum s_i(2|\mathbf{r}_i - \mathbf{x}|/c) \right|^2, \quad (2)$$

where  $\mathbf{x}$  is the position vector in the image. This is a simple imaging process whereby the received signal is shifted by the assumed propagation path length such that all signals are coherently superimposed to focus on the targets. Although most of the imaging methods used for medical imaging assume a bi-static measurement system, for simplicity, we employ a mono-static system with the migration method.

### 3.2. Envelope Method

The Envelope method produces an image as an envelope of ellipses with the foci on the elements [14]. For mono-static measurement data, the image is produced with an envelope of circles, not ellipses. The original Envelope method can be applied only to data measured with a linear element array or a probe scanned linearly. In this section we propose an extended Envelope method and apply it to a concave ultrasound array measurement system.

First, peak points are extracted after applying the matched filter, satisfying

$$\frac{ds_i(t)}{dt} = 0, \quad (3)$$

$$|s_i(t)| > \delta, \quad (4)$$

where  $\delta$  is a positive constant for eliminating noise components. This value  $\delta$  can be chosen based on the standard deviation  $\sigma_n$  of a distribution function of the Gaussian noise model; e.g.  $\delta = 3\sigma_n$ . As we assume a single target in this study, only one peak point is estimated for each  $i$ , and the estimated delay time  $t = T_i$  is uniquely determined.

Next, the method calculates points on the circle with the center point at  $\mathbf{r}_i$  and the radius  $a_i = cT_i/2$ . Points  $\mathbf{x} = \mathbf{x}_{i,k}$  on the circle are calculated as

$$\mathbf{x}_{i,k} = r_0 \begin{pmatrix} \cos \theta_i \\ \sin \theta_i \end{pmatrix} + a_i \begin{pmatrix} \cos \phi_k \\ \sin \phi_k \end{pmatrix}, \quad (5)$$

where the  $i$ -th element is located at  $\mathbf{r}_i = r_0(\cos \theta_i, \sin \theta_i)$ . Then,  $\mathbf{x}_{i,k}$  is transformed into polar coordinates as

$$\mathbf{x}_{i,k} = (x_{i,k}, y_{i,k}) \quad (6)$$

$$\rightarrow (\rho_{i,k}, \psi_{i,k}) = \left( \sqrt{x_{i,k}^2 + y_{i,k}^2} \cdot \tan^{-1} \left( \frac{y_{i,k}}{x_{i,k}} \right) \right). \quad (7)$$

Substituting Eq. (5) into Eq. (7), we obtain

$$\rho_{i,k} = r_0^2 + a_i^2 + 2r_0a_i \cos(\theta_i - \phi_k), \quad (8)$$

$$\psi_{i,k} = \tan^{-1} \left( \frac{r_0 \sin \theta_i + a_i \sin \phi_k}{r_0 \cos \theta_i + a_i \cos \phi_k} \right). \quad (9)$$

Finally, the image surface  $R(\Psi)$  for a convex target in polar coordinates is calculated by solving the following conditional minimization problem

$$R(\Psi) = \min_{i,k} r_0^2 + a_i^2 + 2r_0a_i \cos(\theta_i - \phi_k) \quad (10)$$

$$\text{subject to } \tan^{-1} \left( \frac{r_0 \sin \theta_i + a_i \sin \phi_k}{r_0 \cos \theta_i + a_i \cos \phi_k} \right) = \Psi, \quad (11)$$

where the degree of freedom for the optimization variables  $(i, k)$  is only one in Eq. (10), because of the constraint in Eq. (11). The final image  $S(\mathbf{x})$  is generated by using  $R(\Psi)$  as

$$S(\mathbf{x}) = \begin{cases} A(\Psi) & \text{for all } \mathbf{x} \text{ on } R(\Psi) \\ 0 & \text{otherwise} \end{cases}, \quad (12)$$

where the intensity  $A(\Psi)$  of the image is defined as

$$A(\Psi) = |s(T_{i'})|^2. \quad (13)$$

Here,  $i'$  is the optimum element number  $i$  that minimizes the right-hand side of Eq. (10).

## 4. IMAGING WITH ULTRASONIC MEASUREMENT DATA

In this section, we present the results of applying the two methods to the measured data. The averaged peak S/N is 23.0dB after processing the measured data with the matched filter. Here, this peak S/N is defined as

$$S/N = \frac{\max_{i,t} |s_i(t)|^2}{\frac{1}{TN_e} \sum_i^{N_e} \int_0^T |n_i(t)|^2 dt}, \quad (14)$$

where  $N_e$  is the number of elements employed for imaging,  $s_i(t)$  and  $n_i(t)$  are the echo and noise after applying the matched filter.

First, we show the imaging performance using data measured with the array probe 1 in Fig. 2 out of the three array probes. Figure 4 shows the estimated images with the migration method using 128, 32 and 16 elements of the element array, where 32 and 16 are selected at fixed intervals, i.e. the elements #1, #5, #9,  $\dots$ , #125 are used for imaging with the 32-element array. The image is normalized to the maximum value in the image. The dashed lines show the actual target shape. Numerous undesired artifacts are visible, especially when using a smaller number of elements. Less artifacts are seen when using 128 elements as they are cancelled out in the summation process described by Eq. (2).

Figure 5 shows the received waveforms (solid lines) and the estimated delay time (the dashed line) for each element as given by Eq. (4). Note that the delay time has been smoothly estimated. Figure 6 shows the estimated images produced with the Envelope method using the same data set as shown in Fig. 4. The images are clearer than the images in Fig. 4 and are minimally degraded even when using a small number of elements. This is because the delay time is estimated in the time domain when using the Envelope method, which prevents unwanted interference between echoes.

Figure 7 shows the root mean square (RMS) error of images acquired by the two imaging methods and when using different numbers of elements (8, 16, 32, 64 and 128) to quantitatively evaluate the imaging performance. The RMS error  $e$  is calculated using an image  $S(\mathbf{x})$  as

$$e = \sqrt{\frac{\sum S(\mathbf{x})|\mathbf{x} - \mathbf{c}(\mathbf{x})|^2}{\sum S(\mathbf{x})}}, \quad (15)$$

where  $\mathbf{c}(\mathbf{x})$  is the point on the actual target surface that is closest to the point  $\mathbf{x}$ . The image clearly shows that the

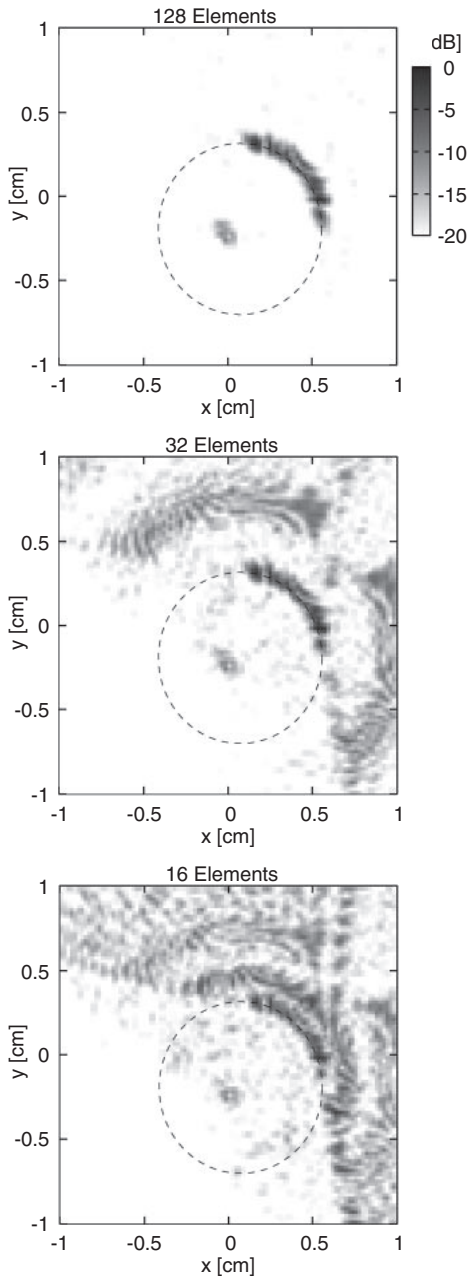


Fig. 4 Estimated images using the migration method.

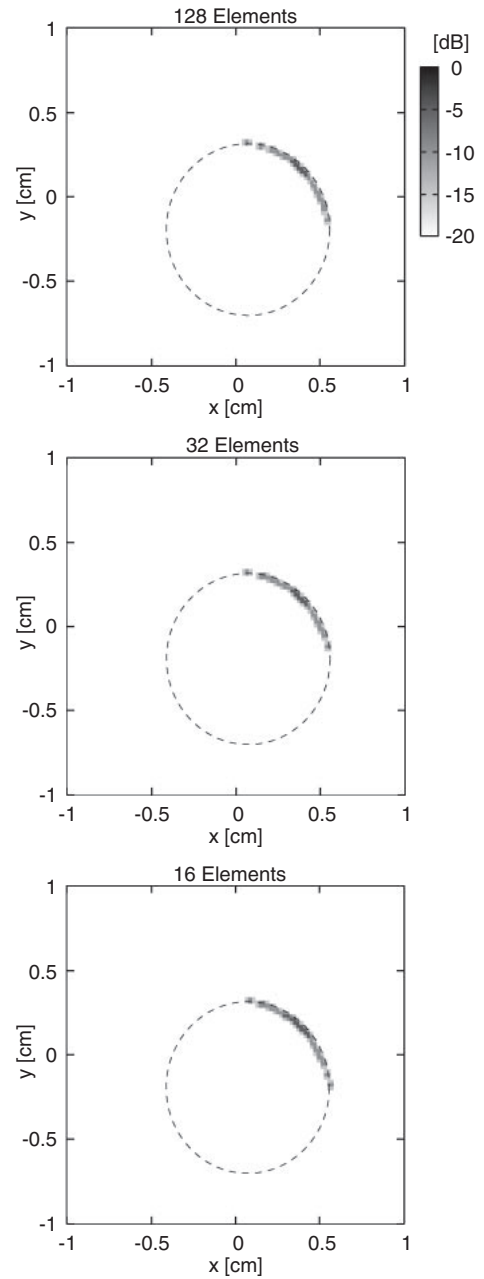


Fig. 6 Estimated images using the Envelope method.

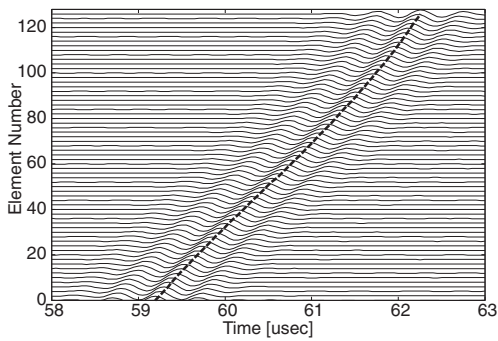


Fig. 5 Estimated delay time for each element.

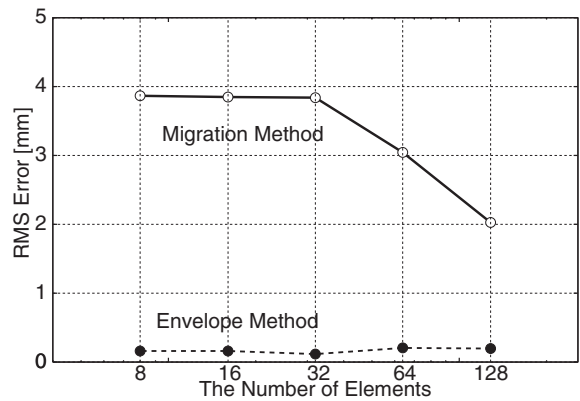
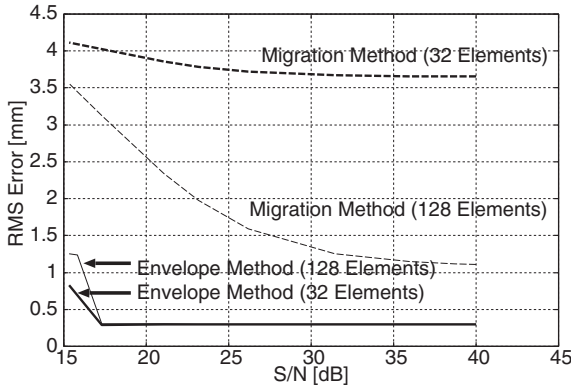


Fig. 7 RMS error for each imaging method when using different numbers of elements (S/N = 23.0 dB).



**Fig. 8** RMS error for peak S/N.

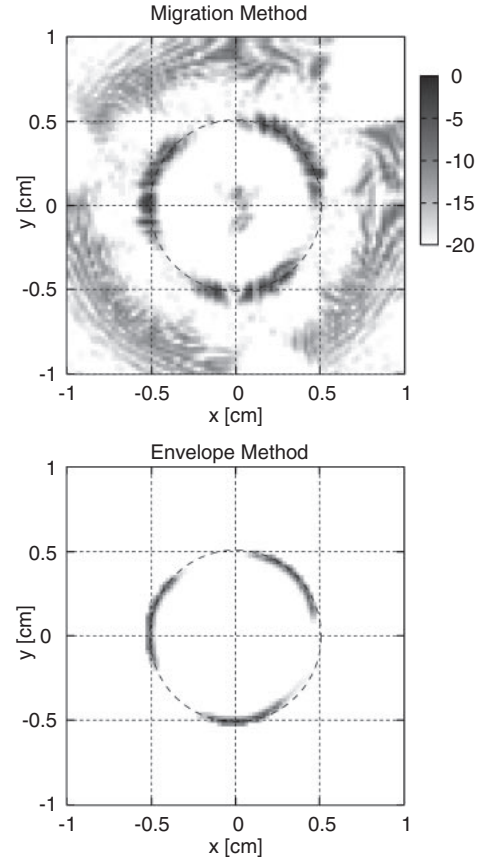
Envelope methods suppresses artifacts and retains the capability for accurate imaging even when employing a small number of elements.

Figure 8 shows the relationship between the RMS error and the peak S/N. The RMS error for the migration method is larger than 1.0 mm even for S/N = 40 dB, while the Envelope method gives accurate images with an RMS error less than 0.5 mm for S/N > 17 dB. The RMS error for the migration method using 32 elements has a floor around 3.6 mm and does not improve even for a higher S/N because the artifacts in the image are not caused by the noise, but by interference between different echoes. The RMS error for the Envelope method is not sensitive to the number of elements because the number of elements determines the resolution and has little effect on accuracy.

We have applied the imaging methods to the data measured with only one of the three array probes. The images obtained with three array probes are shown in Fig. 9 to demonstrate the imaging performance. The imaging process for each array is the same as that explained above. The number of elements for each probe is set to 32. Using three array probes, a wider range of the target shape is imaged. It is verified that the Envelope method outperforms the migration method with a reduced number of elements and using three array probes. The RMS error values are 3.5 mm and 0.31 mm for the migration and Envelope methods.

## 5. COMPARISON WITH ADVANCED METHOD

In the previous sections, we investigated the performance of the proposed method by comparing it with the migration method only. However, the migration method is not specifically designed for medical ultrasonic imaging. In medical imaging, both the media and targets are inhomogeneous, and they generate speckle noise. To address this problem, the wavelet-based frequency decomposition imaging method was proposed by Cincotti *et al.* [21]. This



**Fig. 9** Estimated images with three array probes using migration and Envelope methods.

method employs wavelet packets (WP) to decompose signals into multiple sub-band signals, and is one of the frequency compounding imaging methods. The frequency compounding imaging has already been clinically applied and reported to be effective [22].

We apply the WP decomposition imaging method to our signals to verify the performance. The parameters are the same as in [21], where four-level WP decomposition is assumed using a Daubechies db3 wavelet to decompose each signal into sixteen sub-band signals. Next, a soft threshold algorithm is applied to these wavelet components, where the threshold  $t_h = s_e \sqrt{2 \log_2 N}$  is determined with a data length  $N = 512$  and a risk-related parameter  $s_e = 0.1$ . Finally, using the migration method, sixteen reconstructed signals are used to generate sixteen images, which are incoherently summed to produce the final image.

The solid and broken lines in Fig. 10 represent the sixteen sub-band waveforms and filtered ones, respectively, where the scales are denoted by numbers, with the lowest and highest frequency sub-bands corresponding to 1 and 16, respectively. Large components are localized to a few scales, while other small components are suppressed with the nonlinear filter.

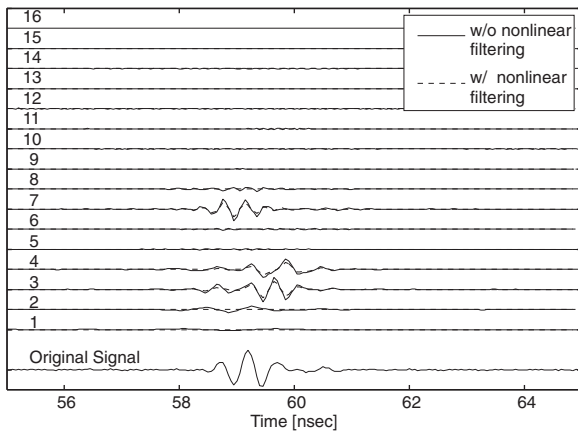


**Fig. 10** Waveforms decomposed using wavelet packets with and without nonlinear filtering.

Figure 11 shows the images estimated using the WP decomposition imaging method. The target shape can be estimated in these images despite them being blurred because of the incoherent summation of sub-band images. The RMS error values are 1.37 mm, 3.56 mm and 3.58 mm for 128, 32, and 16 elements, respectively. Incoherent summation was introduced to suppress speckle noise caused by the inhomogeneity of the media. In our case, however, the media is assumed to be homogeneous, so the sub-band decomposition method does not contribute to suppressing artifacts in the images.

## 6. DISCUSSION

A method to reduce the number of ultrasound elements for monitoring liquid flow in a pipe has been proposed by Yang *et al.* [23] who introduced a non-linear thresholding technique. This technique varies the threshold to remove image artifacts depending on the distance between the element and the pixel position. However, it requires the determination of two parameters that consider image quality, which is not always an easy task. In this paper we have presented another method for reducing the number of elements while maintaining a high level of imaging accuracy.

As mentioned in Section 3.1, the assumed imaging model is based on a mono-static measurement system, not a bi-static one. Considering that bi-static measurements are typically used for medical imaging, an important future task will be to compare the performance of the two imaging methods using data acquired with a bi-static measurement.

The results in this paper do not guarantee that our proposed method is effective for any arbitrary targets. For example, to apply the proposed method to medical imaging, other hard problems need to be resolved, since both the media and targets for medical imaging are inhomogeneous, which is opposite to our simple model.

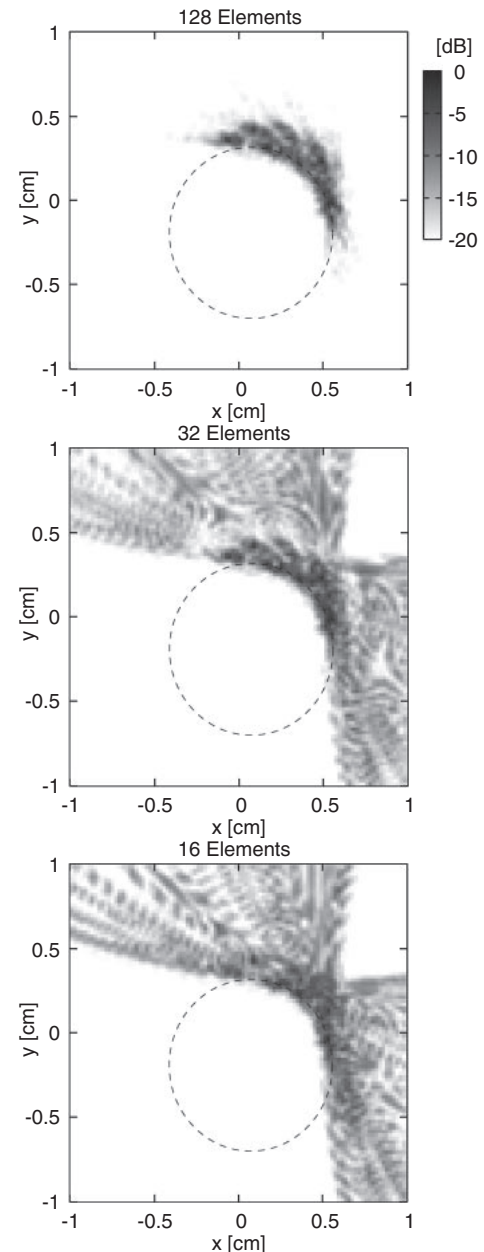


**Fig. 11** Estimated images using the wavelet-based frequency decomposition imaging method.

Additionally, the proposed method has to be extended to estimate concave-shaped targets, because our method was designed assuming only convex-shaped targets. Thus, the proposed method can be considered effective only in certain applications such as industrial inspection for manufacturing, where it is needed to obtain images of simple-shaped convex targets.

## 7. CONCLUSION

We have presented the initial results of an ultrasonic imaging experiment using two imaging methods, the conventional migration method and an extended Envelope method. Each method was applied to ultrasound measure-

ment data acquired with a 128-element concave element array. The results demonstrate that the Envelope method can produce clearer images than the conventional migration method. In addition, the image quality of the Envelope method does not deteriorate when using a smaller number of elements, to as low a number as 16. This finding suggests that by using the Envelope method, a simplified low-cost element array for medical ultrasonic imaging can be realized.

## REFERENCES

- [1] D. Vray, A. Discher, J. Lefloch, W. Mai, P. Clarysse, Q. C. Pham, J. Montagnat and M. Janier, "3D quantification of ultrasound images: Application to mouse embryo imaging in vivo," *Proc. 2002 IEEE Ultrason. Symp.*, Vol. 2, pp. 1597–1600 (2002).
- [2] L. Sun, C. Feng, J. M. Cannata, J. A. Johnson, J. T. Yen and K. K. Shung, "A real-time high frame rate high frequency ultrasonic system for cardiac imaging in small animals," *Proc. 2006 IEEE Ultrason. Symp.*, pp. 2206–2209 (2007).
- [3] L.-J. Xu and L.-A. Xu, "Ultrasound tomography system used for monitoring bubbly gas/liquid two-phase flow," *IEEE Trans. Ultrason. Ferroelectr. Freq. Control*, **44**, 67–76 (1997).
- [4] N. Sponheim, L.-J. Gelius, I. Johansen and J. J. Stamnes, "Quantitative results in ultrasonic tomography of large objects using line sources and curved detector arrays," *IEEE Trans. Ultrason. Ferroelectr. Freq. Control*, **38**, 370–379 (1991).
- [5] T.-O. Müller, R. Stotzka, N. V. Rüter, K. Schlote-Holubek and H. Gemmeke, "3D ultrasound computer tomography: data acquisition hardware," *2004 IEEE Nucl. Sci. Symp. Conf. Rec.*, pp. 2788–2792 (2004).
- [6] K. Nogami and A. Yamada, "Evaluation experiment of ultrasound computed tomography for the abdominal sound speed imaging," *Jpn. J. Appl. Phys.*, **46**(7B), 4820–4826 (2007).
- [7] N. V. Rüter, G. F. Schwarzenberg, M. Zapf and H. Gemmeke, "Improvement of 3D ultrasound computer tomography images by signal pre-processing," *2008 IEEE Int. Ultrason. Symp. Proc.*, pp. 852–855 (2008).
- [8] N. Duric, Li. Cuiping, C. Glide-Hurst, P. Littrup, L. Huang, J. Lupinacci, S. Schmidt, O. Rama, L. Bey-Knight and Y. Xu, "Breast imaging with ultrasound tomography: Clinical results at the Karmanos Cancer Institute," *Proc. Int. Conf. BioMed. Eng. Inf.*, Vol. 2, pp. 713–717 (2008).
- [9] M. Karaman, I. O. Wygant, Ö. Oralkan and B. T. Khuri-Yakub, "Minimally redundant 2-D array designs for 3-D medical ultrasound imaging," *IEEE Trans. Med. Imaging*, **28**, 1051–1061 (2009).
- [10] P. K. Weber, R. M. Schmitt, B. D. Tylkowski and J. Steck, "Optimization of random sparse 2D-transducer arrays for 3D electronic steering and focusing," *Proc. IEEE Symp. Ultrason.*, pp. 1503–1506 (1994).
- [11] G. R. Lockwood and F. S. Foster, "Optimizing the radiation pattern of sparse periodic two-dimensional arrays," *IEEE Trans. Ultrason. Ferroelectr. Freq. Control*, **43**, 15–19 (1996).
- [12] S. Holm, B. Elgetun and G. Dahl, "Properties of the beampattern of weight- and layout-optimized sparse arrays," *IEEE Trans. Ultrason. Ferroelectr. Freq. Control*, **44**, 983–991 (1997).
- [13] S. Kidera, T. Sakamoto and T. Sato, "A robust and fast imaging algorithm with an envelope of circles for UWB pulse radars," *IEICE Trans. Commun.*, **E90-B**, 1801–1809 (2007).
- [14] S. Kidera, T. Sakamoto and T. Sato, "High-resolution and real-time 3-D imaging algorithm with envelope of spheres for UWB radars," *IEEE Trans. Geosci. Remote Sensing*, **46**, 3503–3513 (2008).
- [15] S. Kidera, Y. Kani, T. Sakamoto and T. Sato, "A fast and high-resolution 3-D imaging algorithm with linear array antennas for UWB pulse radars," *IEICE Trans. Commun.*, **E91-B**, 2683–2691 (2008).
- [16] K. Saho, T. Kimura, S. Kidera, H. Taki, T. Sakamoto and T. Sato, "Experimental study of robust and high-resolution ultrasound imaging algorithm with adaptive smoothing techniques," *Proc. Workshop Space Aeronaut. Navig. Electron.* (2008).
- [17] T. Miyashita and A. Honda, "An experimental study of ultrasonic diffraction tomography with circular scanning," *Jpn. J. Appl. Phys.*, **39**(5B), 3101–3102 (2000).
- [18] A. Yamada and K. Kurita, "Transmission-type ultrasonic inverse scattering computed tomography using observation data on circular arc points," *Jpn. J. Appl. Phys.*, **40**(5B), 3890–3895 (2001).
- [19] M. Helbig, M. A. Hein, U. Schwarz and J. Sachs, "Preliminary investigations of chest surface identification algorithms for breast cancer detection," *Proc. IEEE Int. Conf. Ultra-Wideband*, Vol. 2, pp. 195–198 (2008).
- [20] T. Sakamoto and T. Sato, "A target shape estimation algorithm for pulse radar systems based on boundary scattering transform," *IEICE Trans. Commun.*, **E87-B**, 1357–1365 (2004).
- [21] G. Cincotti, G. Loi and M. Pappalardo, "Frequency decomposition and compounding of ultrasound medical images with wavelet packets," *IEEE Trans. Med. Imaging*, **20**, 764–771 (2001).
- [22] B. Mesurrolle, T. Helou, M. El-Khoury, M. Edwardes, E. J. Sutton and E. Kao, "Tissue harmonic imaging, frequency compound imaging, and conventional imaging—Use and benefit in breast sonography," *J. Ultrasound Med.*, **26**, 1041–1051 (2007).
- [23] M. Yang, H. I. Schlaberg, B. S. Hoyle, M. S. Beck and C. Lenn, "Real-time ultrasound process tomography for two-phase flow imaging using a reduced number of transducers," *IEEE Trans. Ultrason. Ferroelectr. Freq. Control*, **46**, 492–501 (1999).

## APPENDIX

The Envelope method described in Section 3.2 is easily extended to a bi-static layout where the elements for transmitting and receiving are not identical. The delay time  $T_{i,j}$  is defined as a delay time for  $i$ -th and  $j$ -th elements as the transmitter and receiver. Points on the ellipse with the focal points on  $\mathbf{r}_i$  and  $\mathbf{r}_j$  with the long axis  $a = cT_{i,j}/2$  is calculated. This ellipse has an inclination angle

$$\Theta_{i,j} = \arg(\mathbf{r}_i - \mathbf{r}_j), \quad (16)$$

long and short axes

$$a_{i,j} = cT_{i,j}/2, \quad (17)$$

and

$$b_{i,j} = \frac{1}{2} \sqrt{c^2 T_{i,j}^2 - |\mathbf{r}_i - \mathbf{r}_j|^2}, \quad (18)$$

respectively. Any point  $\mathbf{x}$  on the ellipse satisfies

$$(\mathbf{x} - \bar{\mathbf{r}}_{i,j})^T R^T(\Theta_{i,j}) A_{i,j} R(\Theta_{i,j}) (\mathbf{x} - \bar{\mathbf{r}}_{i,j}) = 1, \quad (19)$$

where  $R(\ )$  is the rotation matrix,

$$R(\Theta_{i,j}) = \begin{pmatrix} \cos \Theta_{i,j} & -\sin \Theta_{i,j} \\ \sin \Theta_{i,j} & \cos \Theta_{i,j} \end{pmatrix}, \quad (20)$$

$\bar{\mathbf{r}}_{i,j} = \frac{\mathbf{r}_i + \mathbf{r}_j}{2}$  and the diagonal matrix

$$A_{i,j} = \begin{pmatrix} 1/a_{i,j}^2 & 0 \\ 0 & 1/b_{i,j}^2 \end{pmatrix} \quad (21)$$

are defined. Note that the original Envelope method [14] assumed a linear element array, corresponding to the setting  $\Theta_{i,j} = 0$  for all  $i$  and  $j$  because all the elements  $\mathbf{r}_i$  are on the same straight line. The algorithm described above is a natural extension of the original method, and is obtained by generalizing the layout of elements so as to not be restricted to only a circular array.

The  $k$ -th point  $\mathbf{x} = \mathbf{x}_{i,j,k}$  that satisfies Eq. (19) is calculated, and then transformed into polar coordinates to obtain data sets  $(\psi_{i,j,k}, \rho_{i,j,k})$ . Finally, the estimated shape  $R(\Psi)$  is calculated as

$$R(\Psi) = \min_{i,j,k} \rho_{i,j,k}, \quad (22)$$

$$\text{subject to } \psi_{i,j,k} = \Psi. \quad (23)$$



**Takuya Sakamoto** received his B.E. degree from Kyoto University in 2000, and M.I. and Ph.D. degrees from the Graduate School of Informatics, Kyoto University in 2002 and 2005. He is an assistant professor in the Department of Communications and Computer Engineering, Graduate School of Informatics, Kyoto University. His current research interest is in imaging algorithms for ultra wide-band radar and ultrasound systems. He is a member of the IEICE, the IEEJ and the IEEE.



**Hirofumi Taki** received a M.D. degree from Kyoto University in 2000, a Ph.D. degree in informatics from Kyoto University in 2007, and is presently a research staff at Kyoto University. He has worked on development of the spatial resolution and calcification detection ability in Ultrasonography. Acoustic Society of Japan, IEEE, Japan Society of Ultrasonics in Medicine, IEICE member.



**Toru Sato** received his B.E., M.E., and Ph.D. degrees in electrical engineering from Kyoto University, Kyoto, Japan in 1976, 1978, and 1982, respectively. He is currently a Professor at Graduate School of Informatics, Kyoto University. His major research interests include system design and signal processing aspects of UWB radars and radar remote sensing of the atmosphere.